INTERNATIONAL JOURNAL OF REMOTE SENSING
2020, VOL. 41, NO. 10, 3761–3783
https://doi.org/10.1080/01431161.2019.1711241

Taylor & Francis
Taylor & Francis Group

Check for updates

Assessing the relationship between vegetation greenness and surface temperature through Granger causality and Impulse-Response coefficients: a case study in Mexico

Yunuen Reygadas[a], Jennifer L.R. Jensen[a], Gretchen G. Moisen[b], Nate Currit[a] and Edwin T. Chow[a]

[a]Department of Geography, Texas State University, San Marcos, TX, USA; [b]USDA Forest Service, Rocky Mountain Research Station, Ogden, CO, USA

ABSTRACT

The existence of a consistent inverse relationship between vegetation greenness and surface temperature has been the premise of many environmental studies. However, some authors have found that the nature of this relationship varies depending on the spatial and temporal scales of analysis as well as vegetation type. Therefore, this research aims to contribute to the understanding of this matter by evaluating the annual and intra-seasonal relationship between Leaf Area Index (LAI) and Land Surface Temperature (LST) in Central Mexico using monthly anomalies of Moderate Resolution Imaging Spectroradiometer (MODIS) data collected from 2002 to 2017. LAI is proposed as an alternative index to overcome the shortcomings of other widely used indicators of vegetation greenness (e.g. Normalized Difference Vegetation Index and Enhanced Vegetation Index). The presence/absence of any relationship is investigated through the notion of Granger causality, while the sign and strength of the relationship is estimated by means of an Impulse-Response (IR) function. Unlike traditional regression and correlation analysis, the Granger causality approach enables the examination of lagged effects of one variable over the other based on past values of both variables. IR coefficients, which have been rarely used in the related literature, help to model the over-time response of a variable with the change of another variable. The overall results indicate that, at any temporal scale, Granger causality from LST to LAI occurs more consistently than causality in the opposite direction. At the annual scale, the nature of the relationship is primarily inverse in both directions and usually weaker from LAI to LST. At the seasonal scale, the occurrence of LST to LAI causality is higher in spring (it occurs in about 40% of the evaluated pixels) and lower in winter (10%) among all forest types. The effect of LST on LAI is predominantly inverse (median coefficient 1 month after impulse −0.043) and particularly strong in deciduous broadleaf forest during summer. On the other hand, the effect of LAI on LST is mainly direct in autumn and inverse in the remaining seasons, except for evergreen needleleaf forest where the effect is inverse only in summer. The highest presence (23%) and strength (−0.039) of LAI to LST causality occur in spring over deciduous broadleaf forest. Based on these results, caution has to be

ARTICLE HISTORY
Received 14 May 2019
Accepted 4 November 2019

CONTACT Yunuen Reygadas y_r49@txstate.edu Department of Geography, Texas State University, 601 University Drive, San Marcos, Texas 78666, USA

© 2020 Informa UK Limited, trading as Taylor & Francis Group

exercised when assuming a consistent strong inverse relationship between vegetation greenness and surface temperature, which seems to be the general consensus in much of the literature that makes use of these two variables to study an environmental phenomenon.

1. Introduction

Many environmental studies have successfully accomplished their objectives, such as detecting ecosystem disturbances (Mildrexler et al. 2007; Coops, Wulder, and Iwanicka 2009; Mildrexler, Zhao, and Running 2009), classifying land covers (Ehrlich and Lambin 1996; Roy, Kennedy, and Folving 1997), identifying land cover changes (Lambin and Ehrlich 1996, 1997), monitoring drought (Wan, Wang, and Li 2004), or studying urban heat islands (Weng, Lu, and Schubring 2004), by assuming a constant inverse relationship between vegetation greenness and surface temperature. This assumption, where vegetation greenness is the cause and surface temperature is the effect, lies on the fact that increased amounts of vegetation augment latent heat losses through transpiration, which provokes a reduction in surface temperature (Goward, Cruickshanks, and Hope 1985). However, some authors have demonstrated that the nature of this relationship is not always inverse and that it varies depending on the season, forest type, and spatial scale of analysis (Kaufmann et al. 2003; Zhou et al. 2003; Liu et al. 2006; Notaro, Liu, and Williams 2006; Julien and Sobrino 2009).

Individually, vegetation greenness, commonly measured by multi-spectral sensors through spectral indices such as the Normalized Difference Vegetation Index (NDVI), reveals the conditions of vegetative covers and responds to regional climatic characteristics (Global Observing System for Climate 2019); while surface temperature, often acquired from thermal infrared satellite measurements, is defined as the skin temperature of the ground and is mostly a result of albedo, vegetation cover, and soil moisture (Global Observing System for Climate 2019; Eagleson 2011). Thus, any fluctuation in climatic variables, including surface temperature, affects vegetation greenness after a certain time lag and, in turn, these vegetation changes cause a modification of surface temperature (Notaro, Liu, and Williams 2006).

This relationship between vegetation greenness and surface temperature has been examined by comparing single-date datasets through correlation analysis (Goward, Cruickshanks, and Hope 1985; Kumar and Shekhar 2015) and regression models where surface temperature is the dependent variable (Yue et al. 2007). These studies have found a significant inverse relationship. However, multi-temporal studies have revealed more diverse patterns. By means of regression analysis, Julien and Sobrino (2009) found that in boreal areas the relationship between NDVI and Land Surface Temperature (LST) is clearly direct, while in semi-arid areas is clearly inverse. Through correlation analysis that allows for the examination of non-instantaneous effects of one variable over the other, Kaufmann et al. (2003) reported that in North America the effect of vegetation on surface temperature is mostly inverse during summer, generally direct during winter and spring, and not statistically significant during autumn. Liu et al. (2006) found that vegetation variability is mostly driven by temperature in northern mid and high latitudes; although, vegetation also imposes a direct effect on temperature. Similarly, Zhou et al. (2003)

reported that temperature changes accounted for the largest fraction of NDVI change between the early 1980s and the late 1990s in North America and Eurasia. Notaro, Liu, and Williams (2006) described a significant instantaneous influence of temperature on vegetation over the United States of America, but also a non-instantaneous direct effect of vegetation (leading by 1 month) on temperature, especially during spring and over northern states.

The Granger causality approach has been used to examine the lagged effects of vegetation greenness on surface temperature or vice versa (e.g. Kaufmann et al. 2003; Wang et al. 2006, 2007; Jiang, Liang, and Yuan 2015; Papagiannopoulou et al. 2017), but the use of Impulse-Response (IR) coefficients to explore the sign and strength of this relationship is rare in the literature (e.g. Wang et al. 2007). The Granger causality concept is based on the idea of predictability. When the interaction is studied from vegetation greenness to surface temperature, the Granger causality test attempts to predict surface temperature based on past values of surface temperature and vegetation greenness. If the prediction is improved after including the vegetation greenness values, then vegetation greenness is said to Granger-cause surface temperature (Granger 1969; Jiang, Liang, and Yuan 2015; Papagiannopoulou et al. 2017), but the sign and strength of the causality is not specified. IR functions can determine the sign and strength by modelling the over-time response of a variable to an impulse (i.e. change) of another variable based on the Wold Moving Average representation of a Vector Autoregressive (VAR) Model (Lütkepohl 2005).

Regardless of the methods, most of the studies that have evaluated the relationship between vegetation greenness and surface temperature, or that have modelled a phenomenon using both variables, have employed NDVI (e.g. Ehrlich and Lambin 1996; Roy, Kennedy, and Folving 1997; Lambin and Ehrlich 1996, 1997; Kaufmann et al. 2003; Zhou et al. 2003; Wan, Wang, and Li 2004; Wang et al. 2006, 2007; Yue et al. 2007; Julien and Sobrino 2009; Jiang, Liang, and Yuan 2015; Papagiannopoulou et al. 2017) or Enhanced Vegetation Index (EVI; e.g. Mildrexler et al. 2007; Coops, Wulder, and Iwanicka 2009; Mildrexler, Zhao, and Running 2009) as the vegetation indicator. However, these indices have some disadvantages. NDVI is very sensitive to background brightness in areas with sparse vegetation and saturates in zones with high biomass, while EVI tends to present relatively low values in all biomes and is sensitive to topographic conditions (Huete et al. 2002; Matsushita et al. 2007). Therefore, this study proposes to explore the performance of Leaf Area Index (LAI) as an alternative vegetation greenness indicator. In coniferous canopies, LAI is defined as the total surface area of just one half of all needles per unit ground area; while in broadleaf canopies, it is described as the total one-sided area of all green leaves per unit ground area (Myneni et al. 2002). LAI is then a measure of the amount of vegetation vertically distributed. It can also be considered a measure of the surface potentially available for photosynthesis and as a proxy of the three-dimensional conditions of vegetation.

Thus, this paper aims to contribute to the understanding of the relationship between vegetation greenness and surface temperature by evaluating the annual and intra-seasonal relationship between LAI and Land Surface Temperature (LST) across forest types of Central Mexico. On a pixel-by-pixel basis, the presence of any relationship is investigated through the notion of Granger causality, while the sign and strength of the relationship is estimated by means of an IR function. The procedures are performed using monthly anomalies of Moderate Resolution Imaging Spectroradiometer (MODIS) data collected from 2002 to 2017.

2. Data and methods

2.1. Study area

The study area comprises all 1-km pixels of the MODIS tile h08v06 that were covered by forest during at least 1 year between 2002 and 2017 according to the MODIS Terra + Aqua yearly Land Cover product (MCD12Q1, type 3; Figure 1(a)). These pixels extend over 88,824 km^2 and are mainly distributed over the *Sierra Madre Occidental* (west mountain range) and *Sierra Madre Oriental* (east mountain range). The altitudinal range goes from sea level to 3,363 m with a mean of 1,046 m and a standard deviation of 741 m (Figure 1(b)). The slopes range from 0° to 35° with a mean of 6.9° and a standard deviation of 4.8°.

Tropical climates dominate the region (Figure 1(c)). Forty percent of the study area experiences tropical climate and 34% semi-tropical, whose mean annual temperatures exceed 22°C and 18°C, respectively. Temperate climate extends over 13% of the study area and, in comparison with tropical climates, occurs at higher average elevations where the mean annual temperature oscillates between 12°C and 18°C. Arid climate is generally found towards continental areas and extends over 8% of the study area. Semi-cold climate, whose mean annual temperature oscillates between 5°C and 12°C, occurs at the highest elevations and covers the remaining 3% of the study area. As for precipitation regimes, the rainy season (also called 'the warm half of the year') of most of the study area starts in May and ends in October, which coincides with the emergence and senescence of leaves, respectively (García 2004).

The study area is composed of 61% deciduous broadleaf forest, 35% evergreen broadleaf, and 4% evergreen needleleaf (Figure 1(d)). These forests are composed of a broad range of species (in the order of hundreds). Some of the most frequently found trees are

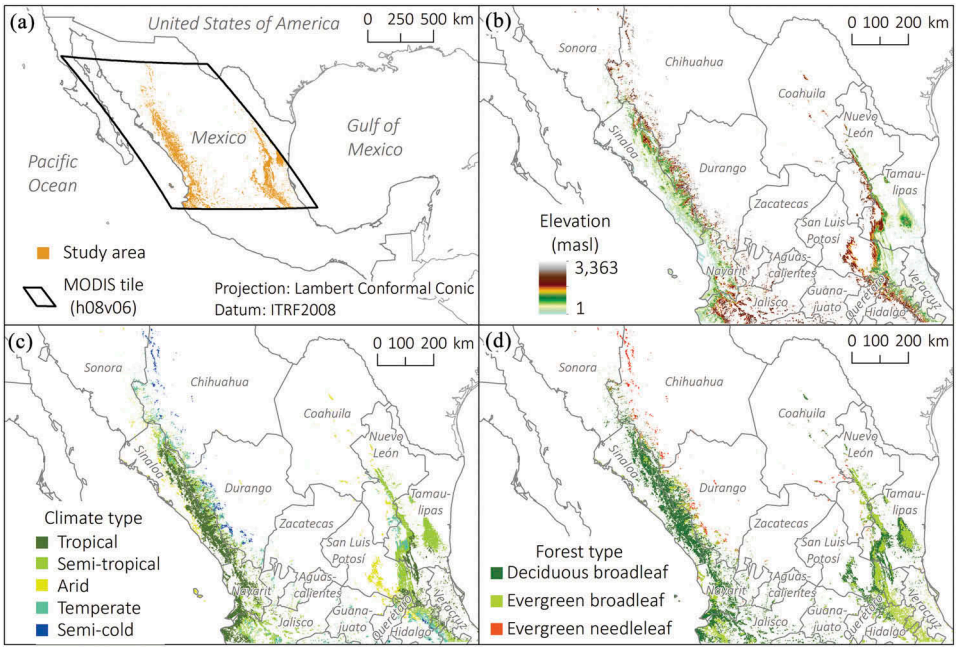

Figure 1. Study area: location (a), elevation (b), climate types (c), and forest types (d).

oaks (e.g. *Quercus magnoliifolia, Quercus rugosa, Quercus laeta, Quercus sideroxyla*), pines (e.g. *Pinus durangensis, Pinus douglasiana*), firs (e.g. *Abies religiosa, Abies durangensis*), mauto (i.e. *Lysiloma divaricatum*), white mangrove (i.e. *Laguncularia racemose*), nance (i.e. *Byrsonima crassifolia*), and bay cedar (i.e. *Guazuma ulmifolia*; CONAFOR 2019).

2.2. Data acquisition and pre-processing

2.2.1. MODIS LST product

The MODIS LST data were downloaded from the Land Processes Distributed Active Archive Centre (LP DAAC) managed by the National Aeronautics and Space Administration's Earth Science Data and Information System (NASA's ESDIS) project. Specifically, MODIS Aqua 8-day LST composites (MYD11A2, Collection 6) of the MODIS tile h08v06 were acquired from 2002 to 2017 at 1-km spatial resolution. Aqua sensor's overpass time, at approximately 1:30 pm above the equator, allows it to capture temperatures close to the daily peak. LST estimates are retrieved from the generalized split window algorithm (Wan and Dozier 1996) or the day/night algorithm (Wan and Li 1997), which use MODIS Thermal Infrared (TIR) data (Wan et al. 2004) and auxiliary MODIS data, such as geolocation, radiance, cloud masking, atmospheric temperature, water vapour, land cover, and snow (Wan 2013). Because TIR signals are not able to penetrate clouds, the LST retrievals are constrained to cloud-free pixels. Wan (2014) reported that the mean LST error of Collection 6 (i.e. the latest version of the MODIS LST product) is within ± 0.6 K and the standard deviation of the validation errors is less than 0.5 K in most validation data sets, which indicates that Collection 6 is an improvement over Collection 5.

All LST composites were projected to Lambert Conformal Conic projection in ITRF2008 datum and clipped to forested areas. To exclude poor quality retrievals, the LST Quality Control (QC) layers were unpacked using the Land Data Operational Product Evaluation (LDOPE) tool. Only LST estimates with an error lower or equal to 2 K were selected to perform the analysis. Based on these good quality retrievals, monthly anomalies of LST were calculated on a pixel-by-pixel basis for each month from January 2002 to December 2017. The anomalies were calculated by subtracting the long-term monthly average, often called climatology, from the monthly means (e.g. anomaly = mean of January 2002—average of all January means of the study period). In order to manipulate the data in an R environment (R Core Team 2018), all LST anomalies were extracted from the raster files and rearranged into a comma-separated values (cvs) file, where each row contains 192 monthly anomalies, which constitute the LST time series of a single pixel.

2.2.2. MODIS LAI product

The MODIS LAI data were also downloaded from the LP DAAC. Specifically, MODIS Terra 8-day LAI composites (MOD15A2H, Collection 6) of the MODIS tile h08v06 were acquired from 2002 to 2017 at 500-km spatial resolution. The early Terra sensor's overpass time, at approximately 10:30 am above the equator, allows it to capture more reliable LAI retrievals due to lower cloud presence (King et al. 2013; Yan et al. 2016). MODIS LAI retrievals are acquired from a radiative transfer model (Knyazikhin et al. 1998) that accounts for vegetation structure. This main algorithm selects the best LAI estimates by comparing measured red and near-infrared spectral values with a look-up table composed of observed spectral values of six biome types and their corresponding LAI values. If

this algorithm fails, a back-up method based on the biome-specific empirical relationship between NDVI and LAI produces the retrievals (Knyazikhin et al. 1998; Myneni et al. 2002; Jensen et al. 2011; Yang et al. 2006; Yan et al. 2016); however, in this study only retrievals from the main algorithm were considered for the analysis.

According to Yan et al. (2016), the latest version of the MODIS LAI product, Collection 6, is considerably better than Collection 5. Collection 6 properly captures the inter-annual variation of LAI and the general seasonality of most biomes, except for evergreen broadleaf forest, for which incorrect seasonal profiles are produced. This issue has been also observed in other satellite products, such as the Carbon cYcle and Change in Land Observational Products from an Ensemble of Satellites (CYCLOPES) and those from the Global Land Surface Satellite (GLASS), and the *Satellite Pour l'Observation de la Terre* (SPOT)-Vegetation GEOV1 system. Therefore, this shortcoming may be difficult to avoid using remotely sensed data.

All LAI composites were projected to Lambert Conformal Conic projection in ITRF2008 datum, resampled to 1-km spatial resolution to make them compatible with the LST data, and clipped to forested areas. During the resampling process, the geo-location was preserved across data products by snapping the raster environment to the cell alignment of the LST datasets. The geo-location is well conserved because the 500-m LAI pixels are originally aligned with the 1-km LST pixels (i.e. one LST pixel perfectly contains four LAI pixels). The LAI QC layers were also unpacked by means of the LDOPE tool and used to select only LAI values obtained from the main algorithm. Then, similar to the procedure performed on the LST data, monthly anomalies of LAI were calculated on a pixel-by-pixel basis for each month from January 2002 to December 2017 and arranged into a cvs file, where each row contains 192 monthly anomalies, which constitute the LAI time series of a single pixel.

2.3. Assessment of the annual and intra-seasonal relationship between LAI and LST

To assess the annual and intra-seasonal relationship between LAI and LST, 86,405 multivariate time series of monthly anomalies of LAI and LST were analysed. These multi-variate time series consist entirely of good quality estimates (Table 1a). For the annual assessment, all values of the time series were used. For the intra-seasonal assessment, the time series were reorganized by season: winter (December–February), spring (March–May), summer (June–August), and autumn (September–November). This means that the three monthly anomalies of a particular season were joined to the three anomalies occurring the following year in the same season. Then, the presence of any relationship between LAI and LST was evaluated in each year-round and season-based multi-variate time series through the Granger causality test. If any relationship was encountered, its sign and strength was estimated by means of an IR function.

2.3.1. Evaluation of Granger causality

The statistical models of the Granger causality approach rely on linear specifications. However, climate-vegetation interactions are non-linear in nature. To solve this inconsistency, this analysis is based on anomalies, which represent deviations from the steady state of the variables and, thus, help to linearly approximate relationships (Glendinning 1994; Wang et al. 2006). It should be noted that the time series of monthly

Table 1. Multi-variate time series that meet the following required criteria: (a) entirely constituted by good quality estimates, (b) stationarity in both variables LAI and LST, and (c) absence of serial autocorrelation at the lag length under analysis. These criteria are additive. Thus, a time series that meets the (c) criterion also meets the (a) and (b) criteria.

			Forest type (total of pixels)			
Criteria			Deciduous broadleaf (64,136)	Evergreen broadleaf (36,233)	Evergreen needleleaf (4,618)	All (104,987)
(a) Good quality			56,561	25,497	4,347	86,405
(b) Stationarity	All year		40,231	16,561	2,728	59,520
	Winter		51,026	22,775	3,874	77,675
	Spring		53,773	22,194	3,423	79,390
	Summer		50,710	22,084	3,848	76,642
	Autumn		50,104	22,548	4,074	76,726
(c) Absence of serial autocorrelation at 1- and 2-month lags	All year	1	37,726	15,297	1,346	54,369
		2	39,428	16,828	2,126	58,382
	Winter	1	50,657	22,646	3,804	77,107
		2	50,869	22,734	3,837	77,440
	Spring	1	53,008	21,449	3,405	77,862
		2	53,659	22,128	3,419	79,206
	Summer	1	50,523	21,987	3,833	76,343
		2	50,655	22,052	3,838	76,545
	Autumn	1	49,738	22,328	4,048	76,114
		2	50,031	22,504	4,072	76,607

LAI and LST anomalies constitute the input data of this analysis; however, to avoid long repetitions, the terms 'monthly' and 'anomalies' may be omitted where the reference is clear.

In formal terms, this section describes the methodology implemented to evaluate the causal relationship between time series of monthly LAI anomalies at a specific pixel and time series of monthly LST anomalies at the same pixel. The existence of causality is examined in both directions. When the interaction is studied from LAI to LST, the test attempts to forecast LST, at a given time, based on past values of LST and LAI. If the prediction of LST is improved when the LAI values are included as predictors, then LAI is said to Granger-cause LST. When the interaction is tested from LST to LAI, the logic is inverse. In both cases, if causality is found, the result should be interpreted as 'predictive causality' rather than 'true causality' (Jiang, Liang, and Yuan 2015; Papagiannopoulou et al. 2017).

A limitation of the Granger causality method is that it cannot be applied to non-stationary time series (i.e. those whose statistical properties, such as mean and variance, do not remain constant over time; Nason 2006) because they are unpredictable and, as a result, cannot be modelled or forecasted (Iordanova 2009). Therefore, prior to examining the causal relationship, a Kwiatkowski-Phillips-Schmidt-Shin (KPSS) test was applied to all LAI and LST time series using the 'urca' R package (Pfaff 2008a). The KPSS test examines the null hypothesis of stationarity around a linear trend at 0.05 significance level (Kwiatkowski et al. 1992). Only stationary time series were considered for the analysis (Table 1b).

Vector Autoregressive (VAR) models were used to derive the predictions required to examine the Granger causality. VAR models are an extension of univariate autoregression models useful to explain and forecast the dynamic behaviour of multi-variate time series (Zivot and Wang 2006). The pixels containing stationary time series of both LAI and LST (Table 1b) were selected to obtain VAR models, which were computed, as well as the rest of the statistical functions of this section, by means of the 'vars' R package (Pfaff 2008a,

2008b). In a VAR model, each variable is a linear function of its own lagged values and the lagged values of the other variables in the model (Mariano et al. 2018). The general form of the VAR (p) model implemented in this study is as follows:

$$\boldsymbol{y}_t = \mathbf{A}_1\boldsymbol{y}_{t-1} + \ldots + \mathbf{A}_p\boldsymbol{y}_{t-p} + u_t, \tag{1}$$

where $\boldsymbol{y}_t$ represents a $K \times 1$ vector of endogenous variables (i.e. variables that are explained by other variables in the system; often called 'depended variables') at time t and u_t assigns a spherical disturbance term (i.e. white noise process) of the same dimension. $\mathbf{A}_1, \ldots, \mathbf{A}_p$ are regression coefficient matrices with a dimension of $K \times K$ and p is the lag length (Pfaff 2008b). The p parameter determines how much of the previous information of all variables (i.e. lag time) is included in the model to predict future behaviours (Wang et al. 2006). In this analysis, y_t is a 2x1 vector of LAI and LST monthly anomalies (i.e. a K = 2), the regression coefficients are $\mathbf{A}_1, \mathbf{A}_2, \mathbf{A}_3$ with a dimension of 2×2, and p is measured in months.

The optimal lag lengths at which the time series should be evaluated were identified by first testing the VAR models using the Akaike Information Criterion (AIC), which finds the lag with enough information content on the two variables without over-fitting (i.e. the best goodness of fit; Zivot and Wang 2006). From this preliminary analysis, the most common optimal lag lengths among all time series were 1 and 2 months. Therefore, the VAR models were repeated two times using these two lags. Then, a Portmanteau test was applied to evaluate the existence of serial correlation in the VAR residuals at a specific lag length. This test examines the null hypothesis of no serial correlation at the significance of 0.05 (Pfaff 2008b). The presence of serial correlation implies that some information (e.g. precipitation, solar zenith angle, aerosol optical depth) is missing in the model to explain the relationship. Thus, only time series with absence of serial correlation were considered for the analysis (Table 1c).

After identifying the appropriate VAR models (i.e. without serial correlation), the existence of Granger causality was tested at 1 and 2-month lags in both directions (i.e. from LAI to LST and from LST to LAI). This means that the test was run twice per lag-length. First, considering LAI as cause and LST as response, and then considering LST as cause and LAI as response. To that end, the vector of LAI and LST monthly anomalies, $\boldsymbol{y}_t$, Equation (1), was split into two sub-vectors as follows:

$$\begin{bmatrix} \boldsymbol{y}_{1t} \\ \boldsymbol{y}_{2t} \end{bmatrix} = \sum_{i=1}^{p} \begin{bmatrix} \alpha'_{11,i} \alpha'_{12,i} \\ \alpha'_{21,i} \alpha'_{22,i} \end{bmatrix} \begin{bmatrix} \boldsymbol{y}_{1,t-i} \\ \boldsymbol{y}_{2,t-i} \end{bmatrix} + \mathbf{CD}_t + \begin{bmatrix} u_{1t} \\ u_{2t} \end{bmatrix}, \tag{2}$$

where $\boldsymbol{y}_{1t}$ and $\boldsymbol{y}_{2t}$ are the sub-vectors, whose dimensions are $(K_1 \times 1)$ and $(K_2 \times 2)$ with $K = K_1 + K_2$, and α is the coefficient of the model. C is the coefficient matrix of potentially deterministic regressors and D_t is the column vector holding the appropriate deterministic regressors. This Granger causality test is an F-type test and is distributed as $F(pK_1K_2, KT - n)$, n being the total number of parameters in Equation (2) and T the number of observations. The null hypothesis, stated as $\boldsymbol{y}_{1t}$ does not Granger-cause $\boldsymbol{y}_{2t}$, is accepted when $\alpha_{21,i} = 0$ for $i = 1, 2, \ldots, p$ and rejected when $\exists\ \alpha_{21,i} \neq 0$ for $i = 1, 2, \ldots, p$ (Pfaff 2008a, 2008b). The test was implemented at 95% confidence level. The rejection of the null hypothesis provides evidence that LAI Granger-causes LST or vice versa, but it does not reveal the sign and strength of the relationship.

2.3.2. Estimation of impulse-response coefficients

To estimate the sign and strength of the relationship between LAI and LST, an IR function was applied to all time series where Granger causality at 1-month lag was found. The IR function measures the over-time response of a variable to an impulse of another variable based on the Wold Moving Average representation of a VAR(p) process (Lütkepohl 2005), which is defined as follows:

$$\boldsymbol{y}_t = \phi_0 u_t + \phi_1 u_{t-1} + \phi_2 u_{t-2} + \ \ldots \ , \tag{3}$$

$\phi_0 = I_k$ and ϕ_s $(s = 1, 2, \ldots)$ can be computed iteratively as indicated below:

$$\phi_s = \sum\nolimits_{j=1}^{s} \phi_{s-j} A_j, \tag{4}$$

where $A_j = 0$ for $j > p$. (i, j)th coefficients of the matrices ϕ_s are interpreted as the expected response of variable $\boldsymbol{y}_{i,t+s}$ to a change in variable $\boldsymbol{y}_{jt}$. Hence, the accumulation of these effects over time $(s = 1, 2, \ldots)$ simulates the impact on variable i after a change in variable j at time s (Pfaff 2008b). In this case, the output of the function consists of IR coefficients calculated for 12 months after a single impulse of LAI or LST.

3. Results

3.1. Annual relationship between LAI and LST

Granger causality was evaluated on 54,369 and 58,382 year-round multi-variate time series that met the required criteria at 1- and 2-month lags, respectively. The results, summarized in Table 2 and Figure 2, indicate that LST Granger-causes LAI in around 80% of the evaluated pixels (grey bar), while LAI Granger-causes LST in no more than 12% of the pixels. In both directions, the presence of causality is slightly higher at 1-month lag. Regarding forest types, causality from LAI to LST occurs in more pixels of evergreen broadleaf forest (8% and 17% at 1- and 2-month lags, respectively), followed by deciduous broadleaf (5% and 10%), and evergreen needleleaf (4% and 7%). In the opposite direction, causality occurs in more pixels of deciduous broadleaf forest (88% and 89%), followed by evergreen needleleaf (71% and 76%), and evergreen broadleaf (65% and 69%).

To examine the nature of the relationship, IR coefficients were calculated for 45,028 and 6,513 pixels that showed Granger causality from LST to LAI and from LAI to LST, respectively, at 1-month lag. The median of those coefficients indicates that Granger causality is primarily inverse in both directions (Figure 3). The response to an impulse of any of the variables is

Table 2. Annual Granger causality at 1- and 2-month lags per forest type. Refer to Table 1c to see the number of pixels that meet all the required criteria and, therefore, were used to evaluate Granger causality.

	Percentage of pixels that show Granger causality			
	From LAI to LST		From LST to LAI	
Forest type	1	2	1	2
Deciduous broadleaf	10	5	89	88
Evergreen broadleaf	17	8	69	65
Evergreen needleleaf	7	4	76	71
All	12	6	83	81

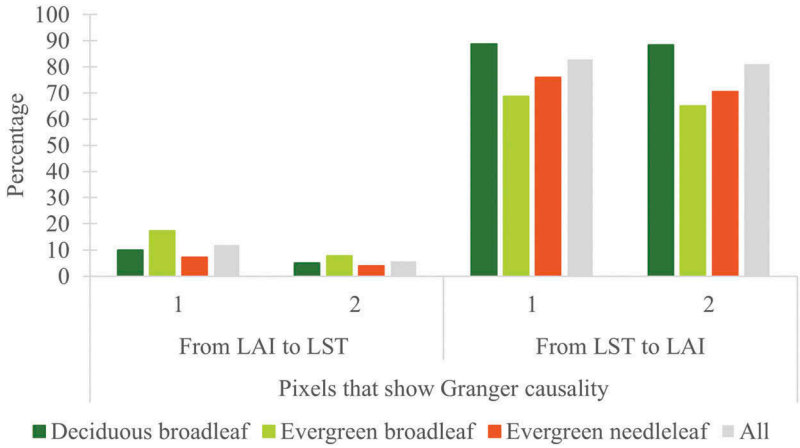

Figure 2. Presence of annual Granger causality at 1- and 2-month lags per forest type.

maximum 2 months after the impulse and then tends to gradually disappear. This means that, based on the annual behaviour of the variables, an increase in, for example, LAI would produce a decrease in LST, which would be most noticeable 2 months after the change in LAI. The effect of LST on LAI is generally stronger than the effect of LAI on LST. The weakest relationship in both directions occurs in evergreen needleleaf forest, while the strongest relationship from LAI to LST is observed in deciduous broadleaf and from LST to LAI in evergreen broadleaf.Figure 4 illustrates the spatial distribution of the IR coefficients calculated for 1 and 2 months after a single impulse of LAI (Figure 4(a)) or LST (Figure 4(b)). Pixels showing causality from LAI to LST concentrate over the east side of the study area, particularly in the States of *San Luis Potosí* and *Tamaulipas*. The effect of LAI on LST is mainly inverse as mentioned before, but there are some pixels in which the relationship is direct. A few coefficients, especially in the east side of the study area, are positive (i.e. direct relationship) the first month and become negative (i.e. inverse relationship) the second month. A few others, especially in the south-western portion, start being negative and become positive the second month (Figure 4(a)). Pixels showing causality from LST to LAI are well represented throughout the study area. The effect of LST on LAI is also predominantly inverse, the strongest inverse effect occurs in the east region 2 months after the LST impulse. However, there are few pixels in which the effect is initially direct and becomes inverse the second month after the impulse, many of these are located in high elevations of both sides of the study area (Figure 4(b)).

3.2. Intra-seasonal relationship between LAI and LST

Granger causality was evaluated at 1- and 2-month lags on all season-based multi-variate time series that met the required criteria (Table 1c). The results, summarized in Table 3 and Figure 5, show that Granger causality from LST to LAI occurs more consistently than Granger causality from LAI to LST in all seasons. If all forest types are considered as a whole (grey bar), the presence of LAI to LST causality is higher in spring (18% and 20% at 1- and 2-month lags, respectively) and lower in summer (5% and 6%). LST to LAI causality is also higher in spring (43% and 40%), but lower in winter (11% and 10%). The highest

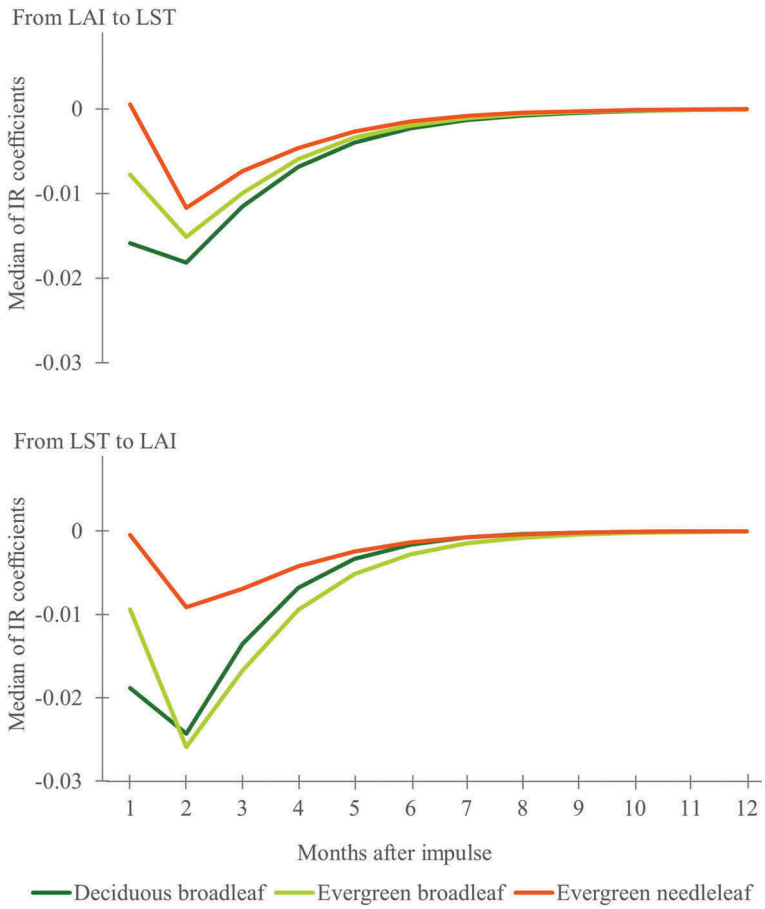

Figure 3. Median IR coefficients of pixels that show annual Granger causality at 1-month lag per forest type.

presence of causality in both directions and all seasons occurs in evergreen needleleaf forest, with the exception of spring and summer for LAI to LST, when deciduous broadleaf and evergreen broadleaf show higher occurrence of causality.

IR coefficients were calculated for all pixels that showed Granger causality at 1-month lag in each season. The median of those coefficients, plotted in Figure 6, revels that the effect of LAI on LST is generally direct in autumn and inverse in the rest of the seasons, except for evergreen needleleaf forest where the effect is direct in winter and spring (Figure 6(a)). The effect of LST on LAI is predominantly inverse across all season, only a slightly direct impact 1 month after the LST change occurs in evergreen broadleaf and evergreen needleleaf forests during winter and autumn (Figure 6(b)). In most cases, the response to change in one of the variables is stronger 2 months after the impulse. In a few cases, such as in summer for deciduous broadleaf (both directions), the strongest impact occurs 1 month after the impulse. In all cases, the effect tends to gradually disappear after the first or second month. The strongest inverse effects of LAI occur in deciduous broadleaf forest during spring and winter, while the strongest direct occurs in evergreen

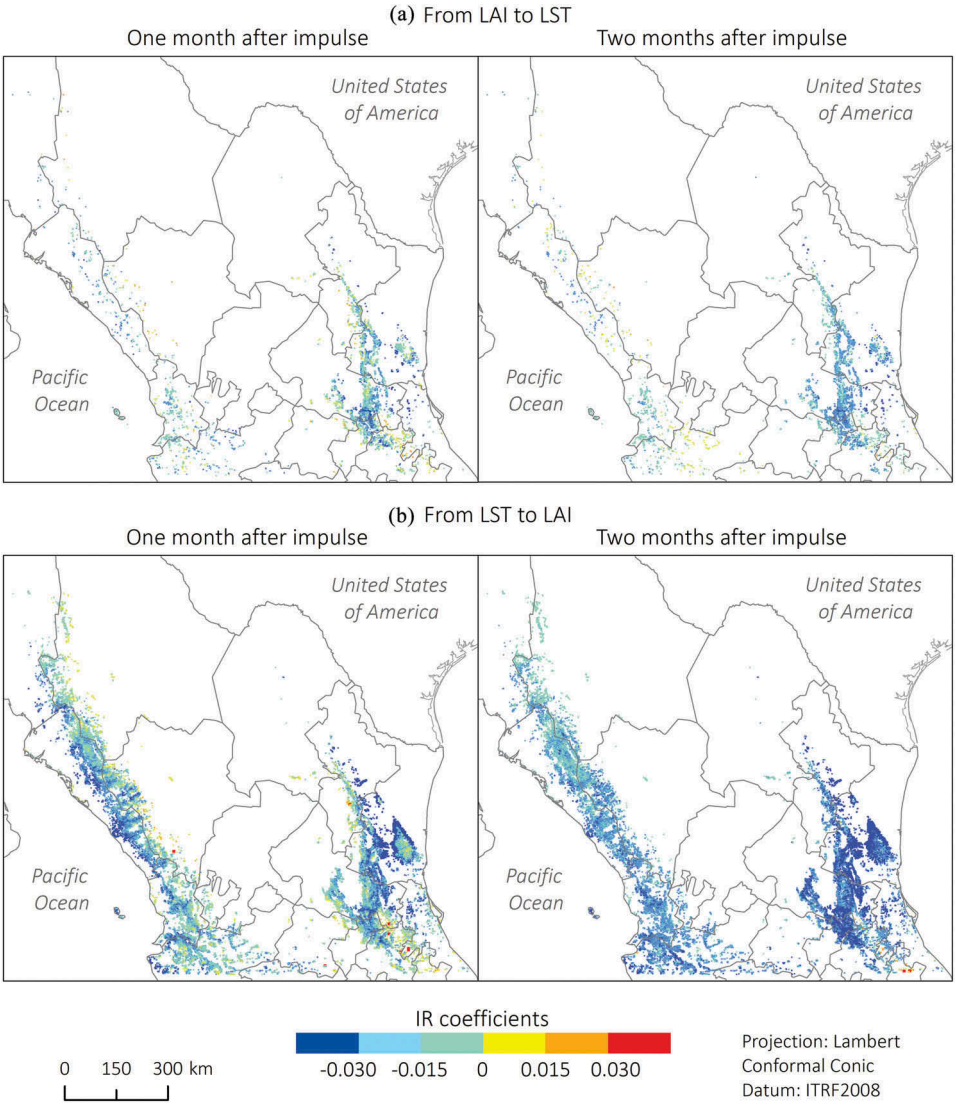

Figure 4. IR coefficients of pixels that show annual Granger causality from LAI to LST (a) or from LST to LAT (b) at 1-month lag.

needleleaf during winter. The strongest effects of LST are all inverse and occur in evergreen broadleaf and deciduous broadleaf during spring and summer, respectively.

The spatial distribution of the IR coefficients calculated for 1 and 2 months after a single impulse of LAI (Figure 7) or LST (Figure 8) shows the diversity of the interactions between the variables. The effect of LAI on LST during winter is primarily direct over the north-western portion and mainly inverse in the remaining area (Figure 7(a)). In spring, the LAI effect is strongly inverse in most pixels, especially 1 month after the impulse. Only a small group of pixels located south-east and north-west of the study area display positive coefficients (Figure 7(b)). In summer, the effect of LAI 1 month after the impulse is predominantly inverse. In the following month, the effect is direct for many of the pixels

Table 3. Seasonal Granger causality at 1- and 2-month lags per forest type. Refer to Table 1c to see the number of pixels that meet all the required criteria and, therefore, were used to evaluate Granger causality.

	Percentage of pixels that show Granger causality															
	From LAI to LST								From LST to LAI							
	Winter		Spring		Summer		Autumn		Winter		Spring		Summer		Autumn	
Forest type	1	2	1	2	1	2	1	2	1	2	1	2	1	2	1	2
Deciduous broadleaf	7	7	23	23	5	6	9	9	10	8	41	37	20	17	17	13
Evergreen broadleaf	5	7	6	16	6	6	7	9	9	10	46	46	13	11	9	9
Evergreen needleleaf	11	8	6	5	3	4	10	12	29	28	47	57	21	17	7	14
All	7	7	18	20	5	6	8	9	11	10	43	40	18	16	14	12

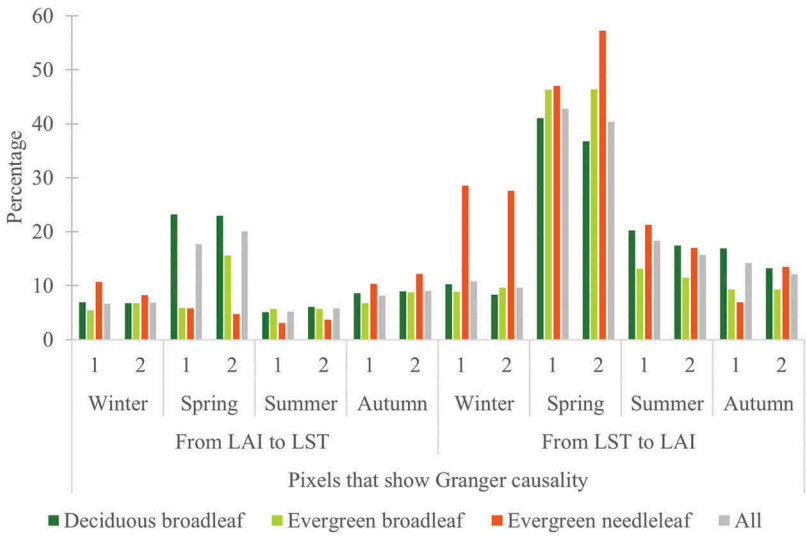

Figure 5. Presence of intra-seasonal Granger causality at 1- and 2-month lags per forest type.

located in the west and north-east. There are cases, such as a small area in the south-west portion of the study area, in which the effect is strongly inverse the first month and becomes strongly direct the second month (Figure 7(c)). During autumn, the effect is weak 1 month after the impulse and becomes primarily direct in the following month, especially in the west portion of the study area (Figure 7(d)).

The effect of LST on LAI presents a wider spatial distribution in all seasons (Figure 8). During winter, the LST effect is generally weak. One month after the impulse, the coefficients are mainly negative at low elevations and primarily positive at high elevations. After 2 months, the coefficients are negative in most of the west side and positive in the majority of the east side (Figure 8(a)). In spring, the effect is predominantly inverse (i.e. negative coefficients) and particularly strong in the eastern portion of the study area (Figure 8(b)). In summer, LST imposes a strong inverse effect on LAI across most of the study area. A notorious exception occurs in pixels located in the State of *Sinaloa*, where the coefficients become highly positive 2 months after the LST impulse (Figure 8(c)). During autumn, the effect is heterogenous. The first month is mainly direct, except for the low altitudes of the

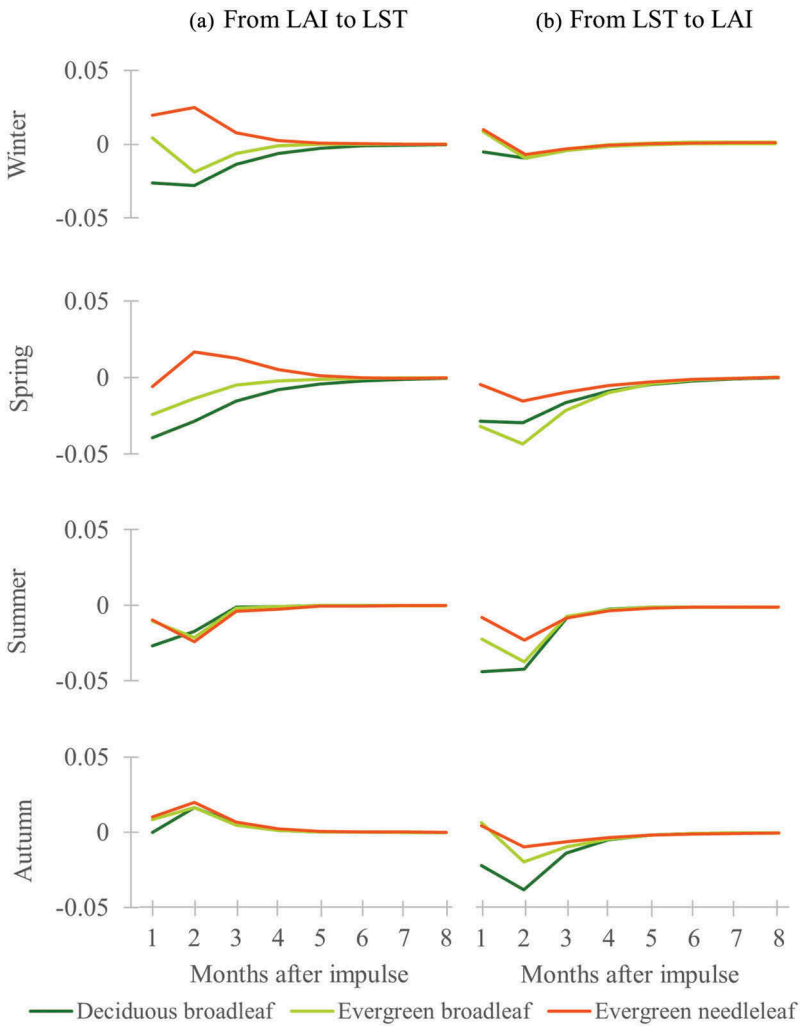

Figure 6. Median IR coefficients of pixels that show intra-seasonal Granger causality from LAI to LST (a) or from LST to LAT (b) at 1-month lag per forest type.

Sinaloa and *Tamaulipas* States. The second month is mostly inverse, except for the south-western portion of the study area, where the coefficients are strongly positive (Figure 8(d)).

4. Discussion

4.1. Relationship between LAI and LST

The results of this research demonstrate that the nature of the relationship between LAI and LST varies depending on the temporal scale. The processes responsible for this variation are not the same at different time scales. Vegetation succession and natural disturbances play a more important role at the annual scale, while phenological changes and climate regimes impose a greater influence at the seasonal scale (Liu et al. 2006).

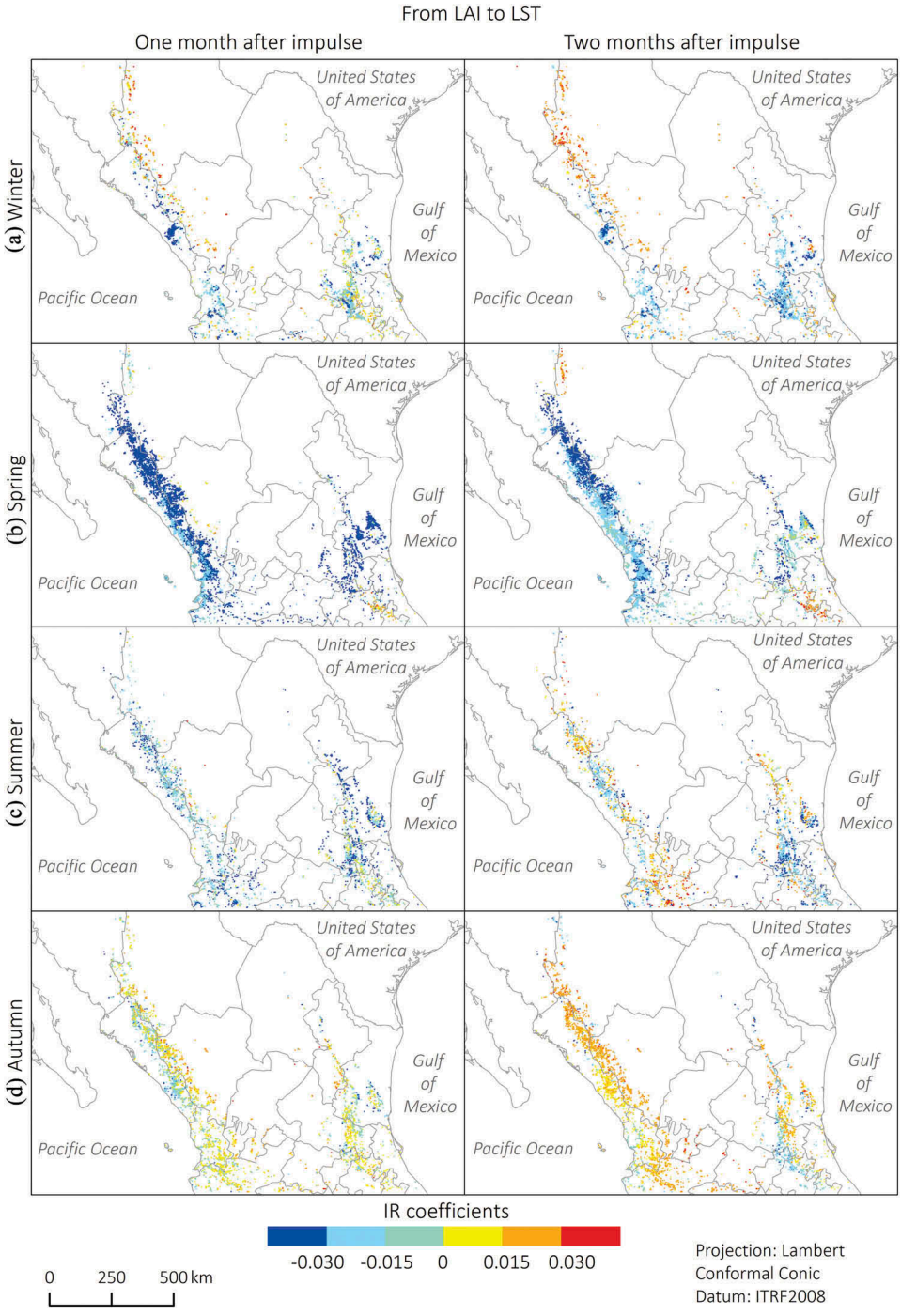

Figure 7. IR coefficients of pixels that show LAI to LST Granger causality at 1-month lag in winter (a), spring (b), summer (c), or autumn (d).

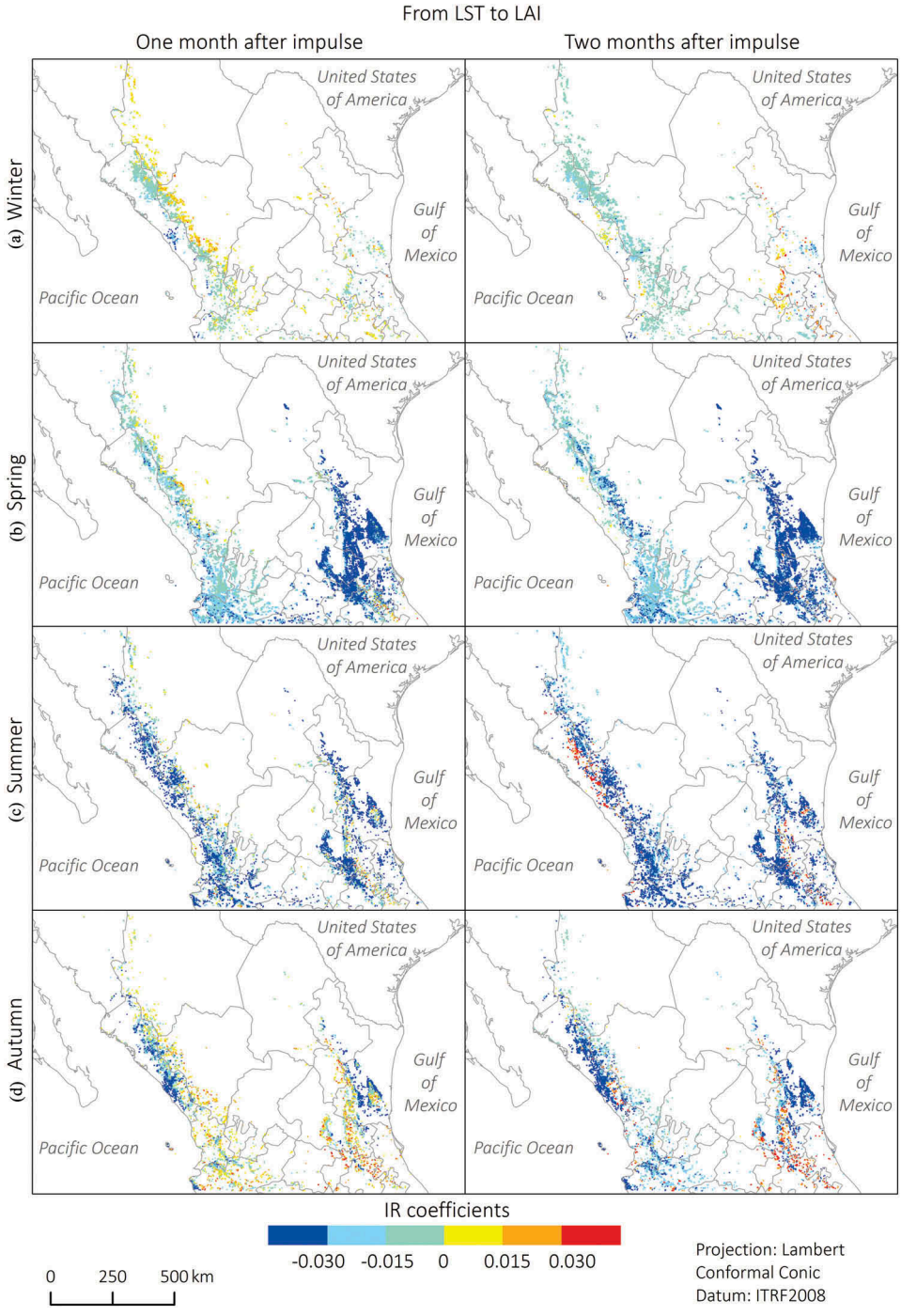

Figure 8. IR coefficients of pixels that show LST to LAI Granger causality at 1-month lag in winter (a), spring (b), summer (c), or autumn (d).

4.1.1. Annual relationship

At the annual scale, LST Granger-causes LAI over most of the study area. In contrast, LAI generally does not Granger-causes LST, except for a portion of the east side of the study area and some small isolated areas over the west side (Figure 4). The nature of the detected causality is primarily inverse in both directions and usually weaker from LAI to LST (Figure 3). These findings are in accordance with Liu et al. (2006), who evaluated feedbacks between Fraction of Photosynthetically Active Radiation (FPAR) and air temperature at a global scale between 1982 and 2000. Using led-lag regression/correlations to identify the presence of interactions and the Frankignoul, Czaja, and L'Heveder (1998) method to estimate the strength of those interactions, they observed a year-round strong inverse correlation from temperature to FPAR over most of the Mexican territory at 1-month lag, but a general absence of correlation from FPAR to temperature. The only area where they detected correlation from FPAR to temperature also exhibits weaker negative coefficients and coincides with the eastern portion where this study found presence of LAI to LST causality (Figure 4).

The existence of a significant effect of surface temperature on vegetation has been similarly addressed by other authors. Zhou et al. (2003) found that fluctuations in temperature accounted for the largest fraction of NDVI change in northern high latitudes between 1982 and 1999. Liu et al. (2006) detected that FPAR variability is predominantly driven by temperature, not only in Mexico, but also in northern mid and high latitudes. Notaro, Liu, and Williams (2006) declared that temperature imposes a significant instantaneous forcing on FPAR over the United States. These results reflect some of the physical process taking place at the land surface. At global and regional scale, surface temperature is a product of several physical drivers (e.g. albedo, soil moisture), of which vegetation is only a moderating factor (Liu et al. 2006; Eagleson 2011). In contrast, vegetation greenness is purely influenced by regional climatic conditions, where temperature is a primary element (Liu et al. 2006; Global Observing System for Climate 2019).

As for forest types (Figure 2), a higher proportion of deciduous broadleaf showed causality from LST to LAI, which demonstrates the general influence of temperature on leaves phenology. LAI to LST causality was observed in more pixels of evergreen broadleaf forest, where fluctuations in temperature are less variable year-round and, therefore, a change in vegetation density may have a more significant impact on the naturally stable surface temperature.

The eastern portion of the study area is characterized by a relatively higher occurrence of LAI to LST causality (Figure 4a) and an inversely stronger effect of LST on LAI (Figure 4b), which can be indicators of more dynamic forest ecosystems. More specifically, these characteristics may suggest vegetation disturbances. According to the Mexico's National Forest and Soils Inventory collected by the *Comisión Nacional Forestal* (CONAFOR), the most common disturbances recorded between 2004 and 2017 on the eastern side are presence of epiphytes, drought, and defoliating insects (in order of importance), while for the western side are fire, logging, and drought (CONAFOR 2019). Among these disturbances, drought has been highlighted as an important driver of forest change. Indeed, in 2009 and 2011, Central Mexico suffered the most severe droughts in seven decades (Domínguez 2016) and, according to CONAFOR (2019), the effects of these droughts have been most severe on the eastern region. Although this study suggests that the distinct behaviour of the LAI and LST variables over the east side of the study area may be

associated with vegetation disturbances, more research must be performed to elaborate on a definitive conclusion.

4.1.2. Intra-seasonal relationship

In all season, Granger causality from LST to LAI occurs more consistently than causality in the opposite direction. The highest and lowest presence of this causality occur in spring and winter, respectively (Figure 5). The effect of LST on LAI is predominantly inverse, generally stronger in summer and weaker in winter (Figure 6). As mentioned in Section 2.1, the rainy period (May–October) is also called the 'warm half of the year' and coincides with the growing season. Therefore, a higher presence of LST to LAI causality in spring suggests that the effect of surface temperature on vegetation greenness is greater during the emergence of leaves than during the senescence. Although the occurrence of causality is lower in summer than in spring, the strongest coefficients are observed in deciduous broadleaf forest during summer, when leaves typically reach maturity. On the other hand, the dry season (November–April), which is also referred to as the 'cold half of the year', is characterized by a lower presence of LST to LAI causality. Thus, colder temperatures are associated with a lower occurrence of causality, which is particularly weak in winter, when the lowest temperatures are reached. These findings are overall in line with what the global scale study of Liu et al. (2006) estimated for Mexico.

Regardless of the season, Granger causality from LAI to LST occurs less commonly than causality in the opposite direction (Figure 5). The effect of LAI on LST is mainly direct in autumn and inverse in the remaining seasons, except for evergreen needleleaf forest where the effect is inverse only in summer (Figure 6). Despite the low presence of this causality, there is a relatively higher occurrence in spring over deciduous broadleaf forest, where LAI imposes a particularly strong inverse effect on LST, which suggests that leaf emergence has a cooling effect on land surface. Kaufmann et al. (2003) also estimated an inverse effect of NDVI on surface temperature for this forest type during spring in Eurasia. Another aspect to highlight is that the strongest direct effect of LAI on LST occurs in winter over evergreen needleleaf. This interaction is also consistent with Kaufmann et al. (2003), who found a strong direct relationship from NDVI to surface temperature in winter over evergreen needleleaf forests of North America and Eurasia. According to these authors, NDVI is not a good indicator of vegetation greenness in winter. Instead, it can be a useful proxy of snow cover extent as these variables are inversely correlated during this season. Thus, a reduction in the extent of snow cover (i.e. an increase in vegetation greenness) increases the absorption of solar radiation and, consequently, raises surface temperature. This process creates a direct correlation from vegetation greenness to surface temperature.

4.2. Challenges and opportunities

This research has a few limitations that can be addressed in future research. First, Granger causality and IR coefficients were estimated using only LAI and LST. However, other variables (e.g. precipitation, solar zenith angle, aerosol optical depth, latitude) may also help to explain the behaviour between vegetation greenness and surface temperature (Kaufmann et al. 2003; Papagiannopoulou et al. 2017). Therefore, the inclusion of additional variables is considered as future step to improve these models. Second, only pixels with stationary time series were considered for the analysis

(Table 1b). However, the exclusion of non-stationary time series may be avoided by detrending those trajectories or by implementing the Toda and Yamamoto (1995) procedure, which allows for the examination of Granger causality in the context of non-stationary data.

Third, there is a false continuity in the season-based time series. For example, the three monthly anomalies of a particular winter were joined to the three monthly anomalies of the following winter. This false seasonal continuity (e.g. winter 2002 and winter 2003) provokes the model to estimate not only relationships occurring among anomalies of the same season, but also between anomalies of a given season and anomalies of the following season. Although, several authors do not discard an interaction between anomalies of different seasons (e.g. Kaufmann et al. 2003; Wang et al. 2006; Kaufmann et al. 2007; Jiang, Liang, and Yuan 2015) and there should not be a reason to discard it *a priori*, this research may be extended to explore an alternative methodology that better handles this false continuity on the season-based time series.

5. Conclusion

On a pixel-by-pixel basis of MODIS imagery, this research evaluated the annual and intra-seasonal relationship between LAI and LST collected from 2002 to 2017 across the forest vegetation of Central Mexico. The Granger causality approach was used detect the presence of any relationship and an IR function was implemented to estimate the sign and strength of the relationship. The main results indicate that, at any temporal scale, Granger causality from LST to LAI occurs more consistently than causality in the opposite direction. At the annual scale, the nature of the relationship is primarily inverse in both directions and usually weaker from LAI to LST. At the seasonal scale, the occurrence of LST to LAI causality is higher in spring and lower in winter. The effect of LST on LAI is predominantly inverse and particularly strong in deciduous broadleaf forest during summer, when leaves typically reach maturity. On the other hand, the effect of LAI on LST is mainly direct in autumn and inverse in the remaining seasons, except for evergreen needleleaf forest where the effect is inverse only in summer. The highest presence of LAI to LST causality occurs in spring over deciduous broadleaf forest, where LAI imposes a particularly strong inverse effect on LST, which suggests that leaf emergence has a cooling effect on land surface.

These results support general conclusions presented in other studies (e.g. Zhou et al. 2003; Liu et al. 2006; Notaro, Liu, and Williams 2006) and reveal novel spatio-temporal patterns of the relationship between vegetation greenness and surface temperature in Central Mexico. As for the input data and methods, this research proposed LAI as an alternative index to overcome the shortcomings of other widely used vegetation greenness indicators (i.e. NDV and EVI). Unlike traditional regression and correlation analysis, the Granger causality approach enabled the examination of lagged effects of LAI on LST, and vice versa. IR coefficients, which have been rarely used in the related literature, helped to model the over-time response of a variable to a change of another variable.

The findings of this research suggest that the relationship between vegetation greenness and surface temperature varies depending on the temporal scale, forest type, and causal variable. Therefore, caution has to be exercised when assuming a consistent inverse relationship driven by vegetation, which seems to be the general consensus in

much of the literature that makes use of these two variables to study an environmental phenomenon (Lambin and Ehrlich 1996, 1997; Wan, Wang, and Li 2004; Mildrexler et al. 2007; Coops, Wulder, and Iwanicka 2009; Mildrexler, Zhao, and Running 2009). Finally, this study is expected to be a contribution to the understanding of vegetation dynamics in Mexico. Based on the results, surface temperature is a significant driver of vegetation greenness in Mexican forests. Therefore, LST products can be considered a potential proxy of vegetation greenness trajectories, especially in the context of a warming climate.

Acknowledgements

This research was supported by the Department of Geography, the Graduate College, and the International Office of Texas State University, as well as by the *Consejo Nacional de Ciencia y Tecnología* (CONACYT). We would like to thank the *Comisión Nacional Forestal* (CONAFOR) for providing us with the National Forest and Soils Inventory Dataset (2004-2017). We also thank the anonymous reviewers for their constructive feedback and suggestions.

Disclosure statement

No potential conflict of interest was reported by the authors.

Funding

This work was supported by the Consejo Nacional de Ciencia y Tecnología and Texas State University.

ORCID

Yunuen Reygadas http://orcid.org/0000-0003-1931-1434
Edwin T. Chow http://orcid.org/0000-0002-0386-5902

References

CONAFOR. 2019. *National Forest and Soils Inventory Dataset, 2004-2017*.

Coops, N. C., M. A. Wulder, and D. Iwanicka. 2009. "Large Area Monitoring with a MODIS-Based Disturbance Index (DI) Sensitive to Annual and Seasonal Variations." *Remote Sensing of Environment* 113 (6): 1250–1261. doi:10.1016/j.rse.2009.02.015.

Domínguez, J. 2016. "Revisión Histórica De Las Sequías En México: De La Explicación Divina a La Incorporación De La Ciencia." *Tecnología Y Ciencias Del Agua* 7 (5): 77–93.

Eagleson, P. S. 2011. *Land Surface Processes in Atmospheric General Circulation Models*. Massachusetts, MA: Cambridge University Press.

Ehrlich, D., and E. F. Lambin. 1996. "Broad Scale Land-Cover Classification and Interannual Climatic Variability." *International Journal of Remote Sensing* 17 (5): 845–862. doi:10.1080/01431169608949051.

Frankignoul, C., A. Czaja, and B. L'Heveder. 1998. "Air–Sea Feedback in the North Atlantic and Surface Boundary Conditions for Ocean Models." *Journal of Climate* 11: 2310–2324. doi:10.1175/1520-0442(1998)011<2310:ASFITN>2.0.CO;2.

García, E. 2004. *Modificaciones Al Sistema De Clasificación Climática De Koppen (Para Adaptarlo a Las Condiciones De La República Mexicana)*. 5th. No. 551.59 G37. Mexico: Instituto de Geografía (UNAM).

Glendinning, P. 1994. *Stability, Instability and Chaos: An Introduction to the Theory of Nonlinear Differential Equations (Vol. 11)*. New York, NY: Cambridge University Press.

Global Observing System for Climate. 2019. "Global Observing System for Climate Essential Climate Variables Data Access Matrix." National Centers for Environmental Information, NOAA. Accessed 10 May 2019. https://www.ncdc.noaa.gov/gosic/gcos-essential-climate-variable-ecv-data-access-matrix

Goward, S. N., G. D. Cruickshanks, and A. S. Hope. 1985. "Observed Relation between Thermal Emission and Reflected Spectral Radiance of a Complex Vegetated Landscape." *Remote Sensing of Environment* 18 (2): 137–146. doi:10.1016/0034-4257(85)90044-6.

Granger, C. W. J. 1969. "Investigating Causal Relations by Econometric Models and Cross-Spectral Methods." *Econometrica: Journal of the Econometric Society* 37 (3): 424–438. doi:10.2307/1912791.

Huete, A., K. Didan, T. Miura, E. P. Rodriguez, X. Gao, and L. G. Ferreira. 2002. "Overview of the Radiometric and Biophysical Performance of the MODIS Vegetation Indices." *Remote Sensing of Environment* 83 (1–2): 195–213. doi:10.1016/S0034-4257(02)00096-2.

Iordanova, T. 2009. "Introduction To Stationary And Non-Stationary Processes". Accessed 03 Jan 2019. http://www.investopedia.com/articles/trading/07/stationary.asp

Jensen, J. L. R., K. S. Humes, A. T. Hudak, L. A. Vierling, and E. Delmelle. 2011. "Evaluation of the MODIS LAI Product Using Independent Lidar-Derived LAI: A Case Study in Mixed Conifer Forest." *Remote Sensing of Environment* 115 (12): 3625–3639. doi:10.1016/j.rse.2011.08.023.

Jiang, B., S. Liang, and W. Yuan. 2015. "Observational Evidence for Impacts of Vegetation Change on Local Surface Climate over Northern China Using the Granger Causality Test." *Journal of Geophysical Research: Biogeosciences* 120 (1): 1–12. doi:10.1002/2014JG002741.

Julien, Y., and J. A. Sobrino. 2009. "The Yearly Land Cover Dynamics (YLCD) Method: An Analysis of Global Vegetation from NDVI and LST Parameters." *Remote Sensing of Environment* 113 (2): 329–334. doi:10.1016/j.rse.2008.09.016.

Kaufmann, R. K., K. C. Seto, A. Schneider, Z. Liu, L. Zhou, and W. Wang. 2007. "Climate Response to Rapid Urban Growth: Evidence of a Human-Induced Precipitation Deficit." *Journal of Climate* 20 (10): 2299–2306. doi:10.1175/JCLI4109.1.

Kaufmann, R. K., L. Zhou, R. B. Myneni, C. J. Tucker, D. Slayback, N. V. Shabanov, and J. Pinzon. 2003. "The Effect of Vegetation on Surface Temperature: A Statistical Analysis of NDVI and Climate Data." *Geophysical Research Letters* 30 (22): 3–6. doi:10.1029/2003GL018251.

King, M. D., S. Platnick, W. P. Menzel, S. A. Ackerman, and P. A. Hubanks. 2013. "Spatial and Temporal Distribution of Clouds Observed by MODIS Onboard the Terra and Aqua Satellites." *IEEE Transactions on Geoscience and Remote Sensing* 51 (7): 3826–3852. doi:10.1109/TGRS.2012.2227333.

Knyazikhin, Y., J. V. Martonchik, R. B. Myneni, D. J. Diner, and W. Running. 1998. "Estimation of Vegetation Canopy Leaf Area Index and Fraction of Absorbed Photosynthetically Active Radiation from MODIS and MISR Data." *Journal of Geophysical Research: Atmospheres* 103 (D24): 32257–32275. doi:10.1029/98JD02462.

Kumar, D., and S. Shekhar. 2015. "Statistical Analysis of Land Surface Temperature-Vegetation Indexes Relationship through Thermal Remote Sensing." *Ecotoxicology and Environmental Safety* 121: 39–44. doi:10.1016/j.ecoenv.2015.07.004.

Kwiatkowski, D., P. C. Phillips, P. Schmidt, and Y. Shin. 1992. "Testing the Null Hypothesis of Stationarity against the Alternative of a Unit Root: How Sure are We that Economic Time Series Have a Unit Root?" *Journal of Econometrics* 54 (1–3): 159–178. doi:10.1016/0304-4076(92)90104-Y.

Lambin, E. F., and D. Ehrlich. 1996. "The Surface Temperature-Vegetation Index Space for Land Cover and Land-Cover Change Analysis." *International Journal of Remote Sensing* 17 (3): 463–487. doi:10.1080/01431169608949021.

Lambin, E. F., and D. Ehrlich. 1997. "Land-Cover Changes in Sub-Saharan Africa (1982-1991): Application of a Change Index Based on Remotely Sensed Surface Temperature and Vegetation Indices at a Continental Scale." *Remote Sensing of Environment* 61 (2): 181–200. doi:10.1016/S0034-4257(97)00001-1.

Liu, Z., M. Notaro, J. Kutzbach, and N. Liu. 2006. "Assessing Global Vegetation-Climate Feedbacks from Observations." *Journal of Climate* 19 (5): 787–814. doi:10.1175/JCLI3658.1.

Lütkepohl, H. 2005. *New Introduction to Multiple Time Series Analysis*. Berlin: Springer Science & Business Media.

Mariano, D. A., C. A. C. Dos Santos, B. D. Wardlow, M. C. Anderson, A. V. Schiltmeyer, T. Tadesse, and M. D. Svoboda. 2018. "Use of Remote Sensing Indicators to Assess Effects of Drought and Human-Induced Land Degradation on Ecosystem Health in Northeastern Brazil." *Remote Sensing of Environment* 213: 129–143. doi:10.1016/j.rse.2018.04.048.

Matsushita, B., W. Yang, J. Chen, Y. Onda, and G. Qiu. 2007. "Sensitivity of the Enhanced Vegetation Index (EVI) and Normalized Difference Vegetation Index (NDVI) to Topographic Effects: A Case Study in High-density Cypress Forest." *Sensors* 7 (11): 2636–2651. doi:10.3390/s7112636.

Mildrexler, D. J., M. Zhao, F. A. Heinsch, and S. W. Running. 2007. "A New Satellite-Based Methodology for Continental-Scale Disturbance Detection." *Ecological Applications* 17 (1): 235–250. doi:10.1890/1051-0761(2007)017[0235:ANSMFC]2.0.CO;2.

Mildrexler, D. J., M. Zhao, and S. W. Running. 2009. "Testing a MODIS Global Disturbance Index across North America." *Remote Sensing of Environment* 113 (10): 2103–2117. doi:10.1016/j.rse.2009.05.016.

Myneni, R. B., S. Hoffman, Y. Knyazikhin, J. L. Privette, J. Glassy, Y. Tian, Y. Wang, et al. 2002. "Global Products of Vegetation Leaf Area and Fraction Absorbed PAR from Year One of MODIS Data." *Remote Sensing of Environment* 83 (1): 214–231. doi:10.1016/S0034-4257(02)00074-3.

Nason, G. P. 2006. "Stationary and Non-Stationary Time Series. Chapter 11." In *Statistics in Volcanology*, edited by Mader H.M., S. G. Coles, C. B. Connor, and L. J. Connor, 129–142. Bath, UK: Geological Society of London.

Notaro, M., Z. Liu, and J. W. Williams. 2006. "Observed Vegetation - Climate Feedbacks in the United States." *Journal of Climate* 19 (5): 763–786. doi:10.1175/JCLI3657.1.

Papagiannopoulou, C., D. Gonzalez Miralles, S. Decubber, M. Demuzere, N. Verhoest, W. A. Dorigo, and W. Waegeman. 2017. "A Non-Linear Granger-Causality Framework to Investigate Climate-Vegetation Dynamics." *Geoscientific Model Development* 10 (5): 1945–1960. doi:10.5194/gmd-10-1945-2017.

Pfaff, B. 2008a. *Analysis of Integrated and Cointegrated Time Series with R*. Second. New York: Springer. ISBN 0-387-27960-1.

Pfaff, B. 2008b. "VAR, SVAR and SVEC Models: Implementation within R Package Vars." *Journal of Statistical Software* 27 (4): 1–32. doi:10.18637/jss.v027.i04.

R Core Team. 2018. R: A language and environment for statistical computing. Vienna, Austria: R Foundation for Statistical Computing. Accessed 10 January 2019. URL https://www.R-project.org/

Roy, D. P., P. Kennedy, and S. Folving. 1997. "Combination of the Normalized Difference Vegetation Index and Surface Temperature for Regional Scale European Forest Cover Mapping Using AVHRR Data." *International Journal of Remote Sensing* 18 (5): 1189–1195. doi:10.1080/014311697218665.

Toda, H. Y., and T. Yamamoto. 1995. "Statistical Inferences in Vector Autoregressions with Possibly Integrated Processes." *Journal of Econometrics* 66: 225–250. doi:10.1016/0304-4076(94)01616-8.

Wan, Z. 2013. "Collection-6 MODIS Land Surface Temperature Products Users' Guide". Institute for Computational Earth System Science, Santa Barbara: University of California.

Wan, Z. 2014. "New Refinements and Validation of the Collection-6 MODIS Land-surface Temperature/emissivity Products." *Remote Sensing of Environment* 140: 36–45. doi:10.1016/j.rse.2013.08.027.

Wan, Z., and J. Dozier. 1996. "A Generalized Split-window Algorithm for Retrieving Land-surface Temperature from Space." *IEEE Transactions on Geoscience and Remote Sensing* 34: 892–905. doi:10.1109/36.508406.

Wan, Z., P. Wang, and X. Li. 2004. "Using MODIS Land Surface Temperature and Normalized Difference Vegetation Index Products for Monitoring Drought in the Southern Great Plains, USA." *International Journal of Remote Sensing* 25 (1): 61–72. doi:10.1080/0143116031000115328.

Wan, Z., Y. Zhang, Q. Zhang, and Z. Li. 2004. "Quality Assessment and Validation of the MODIS Global Land Surface Temperature." *International Journal of Remote Sensing* 25 (1): 261–274. doi:10.1080/0143116031000116417.

Wan, Z., and Z. L. Li. 1997. "A Physics-based Algorithm for Retrieving Land-surface Emissivity and Temperature from EOS/MODIS Data." *IEEE Transactions on Geoscience and Remote Sensing* 35: 980–996. doi:10.1109/36.602541.

Wang, W., B. T. Anderson, D. Entekhabi, D. Huang, Y. Su, R. K. Kaufmann, and R. B. Myneni. 2007. "Intraseasonal Interactions between Temperature and Vegetation over the Boreal Forests." *Earth Interactions* 11 (18): 1–30. doi:10.1175/EI219.1.

Wang, W., B. T. Anderson, N. Phillips, R. K. Kaufmann, C. Potter, and R. B. Myneni. 2006. "Feedbacks of Vegetation on Summertime Climate Variability over the North American Grasslands. Part I: Statistical Analysis." *Earth Interactions* 10 (17): 1–27. doi:10.1175/EI196.1.

Weng, Q., D. Lu, and J. Schubring. 2004. "Estimation of Land Surface Temperature-Vegetation Abundance Relationship for Urban Heat Island Studies." *Remote Sensing of Environment* 89 (4): 467–483. doi:10.1016/j.rse.2003.11.005.

Yan, K., T. Park, G. Yan, Z. Liu, B. Yang, C. Chen, R. R. Nemani, Y. Knyazikhin, and R. B. Myneni. 2016. "Evaluation of MODIS LAI/FPAR Product Collection 6. Part 2: Validation and Intercomparison." *Remote Sensing* 8 (6). doi:10.3390/rs8060460.

Yang, W., D. Huang, B. Tan, J. C. Stroeve, N. V. Shabanov, Y. Knyazikhin, R. R. Nemani, and R. B. Myneni. 2006. "Analysis of Leaf Area Index and Fraction of PAR Absorbed by Vegetation Products from the Terra MODIS Sensor: 2000-2005." *IEEE Transactions on Geoscience and Remote Sensing* 44 (7): 1829–1841. doi:10.1109/TGRS.2006.871214.

Yue, W., J. Xu, W. Tan, and L. Xu. 2007. "The Relationship between Land Surface Temperature and NDVI with Remote Sensing: Application to Shanghai Landsat 7 ETM+ Data." *International Journal of Remote Sensing* 28 (15): 3205–3226. doi:10.1080/01431160500306906.

Zhou, L., R. K. Kaufmann, Y. Tian, R. B. Myneni, and C. J. Tucker. 2003. "Relation between Interannual Variations in Satellite Measures of Northern Forest Greenness and Climate between 1982 and 1999." *Journal of Geophysical Research* 108 (D1): 4004. doi:10.1029/2002JD002510.

Zivot, E., and J. Wang. 2006. "Vector Autoregressive Models for Multivariate Time Series." In *Modeling Financial Time Series with S-Plus®*, 385–429. New York, NY: Springer Science & Business Media.